Citation for published version:
Johnston, DN 2011, 'Numerical modelling of unsteady turbulent flow in tubes, including the effects of roughness and large changes in Reynolds number', *Proceedings of the Institution of Mechanical Engineers, Part C: Journal of Mechanical Engineering Science*, vol. 225, no. 8, pp. 1874-1885. https://doi.org/10.1177/0954406211400795

DOI:
10.1177/0954406211400795

Publication date:
2011

Document Version
Peer reviewed version

Link to publication

©SAGE. The definitive version is available as: Johnston, D. N., 2011. Numerical modelling of unsteady turbulent flow in tubes, including the effects of roughness and large changes in Reynolds number. Proceedings of the Institution of Mechanical Engineers, Part C: Journal of Mechanical Engineering Science, 225 (8), pp. 1874-1885. http://dx.doi.org/10.1177/0954406211400795

University of Bath

Alternative formats
If you require this document in an alternative format, please contact:
openaccess@bath.ac.uk

General rights
Copyright and moral rights for the publications made accessible in the public portal are retained by the authors and/or other copyright owners and it is a condition of accessing publications that users recognise and abide by the legal requirements associated with these rights.

Take down policy
If you believe that this document breaches copyright please contact us providing details, and we will remove access to the work immediately and investigate your claim.

Download date: 05. May. 2023

Numerical modelling of unsteady turbulent flow in tubes, including the effects of roughness and large changes in Reynolds number

D N Johnston

Department of Mechanical Engineering

University of Bath

Abstract

A method has been developed for predicting unsteady turbulent friction in smooth, transitional and rough pipe flow. For transitional and rough pipe flow the effective viscosity at the wall is varied depending on Reynolds number and roughness. An approximation has been made for the transition region by using a cubic spline for the friction factor between the smooth and rough regions.

This turbulence model can be implemented readily in several types of numerical model for pipe flow, including simple lumped parameter models, finite difference/finite element methods and the Method of Characteristics. An approximate method for representing changes in turbulence energy is discussed. Using this, the method is suitable for small and large changes in flow, and for short and long time scales, but further validation is needed.

Keywords

Turbulent flow, unsteady flow, rough pipes, accelerating flow

1. Introduction

A companion paper [1] examines the unsteady friction characteristics of flow in smooth-walled pipes. A numerical approximation was developed based on a model developed by Vardy and Brown [2]. This numerical approximation was shown to be an efficient and accurate representation of Vardy and Brown's physical model. However roughness of the pipe wall is known to have an important effect, particularly for high Reynolds number. In the current paper, the model is extended to include fully rough flow as well as the transition between smooth and rough flow.

It is necessary to determine whether the flow is in the fully smooth region, the fully rough region or a transition region. To do this, appropriate limits between these regions need to be established. From steady friction considerations the turbulent core viscosity and wall viscosity can be estimated. These can then be used in the unsteady friction model.

The unsteady friction model assumes that the turbulence energy and effective viscosity distribution are 'frozen' in time. Whilst this may be true for short time periods, over longer periods the turbulence energy and effective viscosity distribution will change in response to a change in flow. A simple and approximate method is proposed to deal with variations in turbulence.

2. Steady Friction factor

Before friction in unsteady turbulent flow can be considered, it is necessary to understand friction in steady turbulent flow, and this in itself is not clear cut. There have been several studies of friction factor for turbulent flow in rough pipes, and some distinctly different results have been obtained. Schlichting [3] presented a range of friction factor measurements and empirical models. He presented measurements obtained by Nikuradse [4], who used circular pipes with the inside surface covered with tightly packed grains of sand of uniform size. These results are reproduced here in figure 1 (note that $\lambda = 4f$) together with results from Bauer and Galavics [5] for a commercial rough pipe.

Nikuradse's results in figure 1 show a distinct dip between the smooth flow region (lines 2 and 3) and the fully rough region (the horizontal lines at high *Re*). This is rather different to Bauer and Galavics' results which show a gradual, steadily decreasing transition. Apart from Bauer and Galavics' result being for a smaller value of roughness, the difference is attributed to the different nature of the artificial sand roughness and the commercially rough pipe. For the sand the 'roughness density' is very high and the roughness height is very uniform. Moody [6] developed a chart of friction factor for commercially rough pipes which is reproduced in figure 2.

Bauer and Galavics' results for $\frac{R}{k} = 1300$ in figure 1 closely resemble Moody's results, but with an equivalent roughness value $\frac{R}{k_S} = 3600$. That is, the equivalent sand grain size k_S is about 0.35 times the actual estimated roughness k in this case. This difference is probably because of the lower roughness density of the commercially rough pipe, but may also be due to the broader roughness size distribution.

Colebrook [7] developed an equation for friction factor (the *Colebrook-White* equation) which includes the smooth, transition and rough regions and which closely follows the curves on Moody's graph:

$$\frac{1}{\sqrt{4f}} = 1.74 - 2\log\left(\frac{k_S}{R} + \frac{18.7}{Re\sqrt{4f}}\right) \tag{1}$$

The Colebrook-White equation is a good approximation to the friction factors in figure 2, but not to Nikuradse's results in figure 1.

Schlichting [3] stated limits for the smooth, transition and fully rough regions as follows:

Smooth: $0 \le \frac{k_S u_*}{\nu_F} \le 5$

Transition: $5 \le \frac{k_S u_*}{\nu_F} \le 70$ (2)

Fully rough: $\frac{k_S u_*}{\nu_F} > 70$

where u_* is the 'friction velocity', given by $u_* = \overline{u}\sqrt{\frac{f}{2}}$ (3)

and $\frac{k_S u_*}{\nu_F} = \frac{k_S}{R}\frac{Re}{2}\sqrt{\frac{f}{2}}$. (4)

These limits were defined assuming uniform roughness height. For smooth flow the protrusions are fully within the laminar sub-layer. For fully rough flow the resistance is mainly due to the form drag on the protrusions outside of the laminar sub-layer.

Because the Colebrook-White equation does not fit the results in figure 1 well, an alternative method is proposed. Equivalent but simplified equations are used for the fully smooth and fully rough cases as far as the limits given in equations (2), and blending is used in the transition region between the two using a cubic spline.

Fully smooth flow (Blasius' equation): $$\frac{1}{\sqrt{4f}} = 1.74 - 2\log\left(\frac{18.7}{Re\sqrt{4f}}\right) \quad (5)$$

Fully rough: $$\frac{1}{\sqrt{4f}} = 1.74 - 2\log\left(\frac{k_S}{R}\right) \quad (6)$$

For the transition region a cubic spline was applied to $\log_{10}(f)$ with respect to $\log_{10}(Re)$ (logarithms were used because of the broad spread of values). The equations for this are given in Appendix 2.

This is shown in figure 3. Curves representing best fits through Nikuradse's measurements are also shown. Good agreement is obtained between Nikuradse's measurements and the blended model with less than 10% error.

The transition region may be broader for commercially rough pipes because of the broader distribution of roughness heights and the lower density of protrusions. By using a broader transition region, similarly good agreement can be obtained with the Colebrook-White equation. Figure 4 compares the Colebrook-White equation and the blended model using a transition region of $0.02 \le \frac{k_S u_*}{\nu_F} \le 100$. Good agreement is apparent except for the largest roughness values at low *Re*. The lower limit of the transition region is considerably less than the laminar transition of *Re*≈2500 for large roughness values. Nonetheless the same equations are assumed to apply for the calculation of the cubic spline coefficients, although the lower limit is never reached in practice.

Whilst reasonably good agreement can be obtained using this blending method, there is clearly some uncertainty in the limits of the transition region, as well as in the value of the effective roughness k_S. A generic model is therefore only likely to be approximate.

3. Estimation of core and wall viscosities

For the purpose of developing a model for unsteady friction, Vardy and Brown [2, 8] developed a simplified two-region model for turbulent flow. They represented turbulent friction using an effective viscosity that was uniform over the central region (the 'core viscosity') and decreased linearly to the 'wall viscosity' in the outer annulus region. They assumed that the core viscosity was given by the equation

$$\nu_C = N_C R\overline{u}\sqrt{\frac{f}{2}} \tag{7}$$

where $N_C = 0.065$, and the intersection between the core and the outer annulus was at a radius of $0.8R$. This was taken as a crude approximation to a limited number of previously measured viscosity distributions. For smooth pipe flow, the wall viscosity was taken as equal to the fluid's kinematic viscosity, whereas for fully rough flow it was somewhat higher. The estimation of core viscosity for smooth flow is considered in the companion paper [1].

3.1 Fully rough flow

For fully rough flow, the wall viscosity is greater than the fluid viscosity. Vardy and Brown [8] assumed that the core viscosity ν_C is given by equation (7) with $N_C = 0.065$, and the same approach is used here. The friction factor can be estimated using equation (6). It is necessary to determine a value of wall viscosity that is consistent with this friction factor.

Using the two-region model the friction factor is dependent on the wall viscosity and the core viscosity. If the relationship between wall viscosity, core viscosity and friction factor can be determined, the wall viscosity can be estimated as the friction factor and core viscosity are known.

Equation (8) defines the velocity profile for steady flow.

$$\frac{\partial p}{\partial x} = \frac{\rho}{r}\left[\frac{\partial}{\partial r}\left(r\nu(r)\right)\frac{\partial u}{\partial r} + r\nu(r)\frac{\partial^2 u}{\partial r^2}\right] \tag{8}$$

By numerical solution of this equation for arbitrary values of R, ν_C, $\frac{\partial p}{\partial x}$ and ρ, and for a range of values of σ_{CW}, the mean velocity $\bar{u}$ can be determined. This numerical calculation is described in the companion paper [1]. The friction factor can then be determined for any value of σ_{CW}, as follows.

From Darcy's equation,

$$\frac{\partial P}{\partial x} = -\frac{fRe\rho\nu_F\bar{u}}{2R^2} \tag{9}$$

It is assumed that the core viscosity is given by equation (7). This can be rearranged to give equation (10) which relates the core viscosity to the fluid viscosity.

$$\sigma_{CF} = \frac{\nu_C}{\nu_F} = \frac{N_C\bar{u}R}{\nu_F}\sqrt{\frac{f}{2}} = \frac{N_C Re}{2}\sqrt{\frac{f}{2}} \tag{10}$$

Combining (9) and (10) to eliminate ν_F results in equation (11) for f.

$$f = \frac{1}{2}\left(\frac{N_C R^2}{\nu_C\rho\bar{u}}\frac{\partial P}{\partial x}\right)^2 \tag{11}$$

For a range of values of σ_{CW}, $\bar{u}$ can be evaluated numerically, from which f can be found using equation (11). This gives a relationship between f and σ_{CW} which is shown in figure 5.

The value of σ_{CW} can be estimated to within 3% of the calculated points using the polynomial

$$\log_{10}(\sigma_{CW}) = -0.7025[\log_{10}(f)]^3 - 2.9936[\log_{10}(f)]^2 - 5.9431\log_{10}(f) - 3.5609 \tag{12}$$

This information can be used to estimate the core and wall viscosities for a given Reynolds number. Firstly f can be calculated using the Colebrook-White equation for

fully rough flow, equation (6). Secondly the core viscosity ν_C can be estimated using equation (7). Thirdly, σ_{CW} and hence the wall viscosity ν_W can be estimated using equation (12).

3.2 Transitional flow

In the transitional range of Reynolds numbers, the viscosity ratios and N_C need to blend smoothly from the smooth to rough values. The exact form of this transition is not known; however these values should stay within a reasonable range, and in particular σ_{WF} should not be less than 1. Cubic splines could be used in the same way that was proposed for *f*; however this can result in values overshooting the limiting values. Instead, linear interpolation was used for $\log_{10}(\sigma_{WF})$ relative to $\log_{10}(Re)$ (it was also tried for σ_{WF} against *Re*, and the difference was small). Equation (13) can then be used to estimate σ_{CF}, from which σ_{CW} can be calculated. This is the same approximation that was used [1] to obtain σ_{CW} for smooth walled flow, but now allowing for non-unity values of σ_{WF}.

$$\sigma_{CF} = \left(0.1309 \log_{10}\left(\frac{fRe}{\sigma_{WF}} \right) - 0.1119 \right) fRe \tag{13}$$

Several other approaches are possible. For example, the interpolation could be applied to N_C, σ_{CW} or σ_{CF}. Also different forms of interpolation or splines could be used. However this approach guarantees that $\sigma_{WF} \geq 1$. The viscosity ratios and N_C will take different values depending which approach is used, but the overall effect on simulation results will be very small and within the bounds of uncertainty in the value of *f* and limitations of the simple two-region viscosity model.

Figure 6 shows the predicted variation of σ_{CF}, σ_{WF} and σ_{CW} with *Re* for a range of roughness values. The limits of the smooth, transitional and rough regions are marked by symbols, and changes in gradient occur at these points. In the smooth region σ_{CF} and σ_{CW} rise approximately proportionally to *Re*, whilst $\sigma_{WF} = 1$. In the rough region

σ_{CW} is constant and σ_{WF} increases. The transition occurs at higher Reynolds numbers for lower roughness.

4. Turbulence time constant

The development of this method assumes that the turbulence level and effective viscosity distribution are 'frozen' in time. Whilst this may be true for short time periods, over longer periods the turbulence level and effective viscosity distribution will change in response to a change in flow. Brown et al [9] derived an approximate expression for the time constant for turbulence variations. This defines the transition between equilibrium turbulence (low frequency) and invariant turbulence (high frequency). It is given by the equations

$$\tau_B \approx \frac{500R}{u_\infty H}\left(1-\frac{2}{H}\right) \approx \frac{1000R^2}{ReH\nu_F}\left(1-\frac{2}{H}\right)\left(1-\frac{1.5}{H}\right) \tag{14}$$

$$H = 2.2 + \log\left(Re'\sqrt{\frac{f}{2}}\right) \tag{15}$$

u_∞ is the 'free-stream' velocity which Brown et al assumed to be equal to the centre-line velocity. The instantaneous *Re* can be filtered using a low-pass filter with this time constant τ_B to give Re':

$$Re' = \frac{Re}{1+j\omega\tau_B} \tag{16}$$

The friction factor *f* and the viscosity ratio σ_{CW} can then be determined based on this low-pass filtered Re'. However it should be recognised to be very approximate; in reality it may be a non-linear effect and it may not be a first-order filter effect. Nonetheless it is a very useful approximation in the absence of a more rigorous model. It should also be noted that the time constant varies with Reynolds number. The low-pass filtered Re' should be used in equation (15) to calculate *H*. It is not clear whether the instantaneous or filtered Reynolds number should be used in equation (14). This equation derives from the time taken for a particle to travel a

particular distance, and may not be accurate for large velocity changes. The simulation process may be faster and more robust if the filtered Re' is used, as this avoids the possibility of discontinuous changes in the time constant τ_B. However the choice between *Re* or Re' in equation (14) may result in a significant difference in simulation results if the transient involves a large change in *Re*, as will be shown in section 7.

In many cases, the turbulence time constant τ_B will be considerably greater than the period of oscillation of pressure and flow during a transient. The precise value of τ_B will then have little effect on the shape and decay of the transient, but will affect the time taken for the pressure drop and flowrate to reach their new equilibrium levels.

5. Unsteady friction model

In the companion paper [1] an unsteady friction model for smooth laminar flow is described, in which the weighting function coefficients depended on the viscosity ratio σ_{CW}. The same technique can be used for transitional and rough walled flow, the only difference being that $\sigma_{WF} = 1$ for smooth walled flow and $\sigma_{WF} > 1$ for transitional and rough flow. By setting $\sigma_{CF} = \sigma_{WF} = \sigma_{CW} = 1$, this method is also applicable for laminar flow.

It is necessary to convert from normalised weighting functions according to the actual fluid properties.

$$m_k = m_k^* \sigma_{WF} \sqrt{\sigma_{CW}} \tag{17}$$

$$n_k = n_k^* \sigma_{CF} \tag{18}$$

where m_k^* and n_k^* are determined using table 1 and equation (29) of the companion paper [1] according to the current value of σ_{CW}.

$$W_{UE}(j\omega) = \frac{4\nu_F}{R^2} \sum_{k=1}^{K} \frac{m_k j\omega}{\frac{n_k \nu_F}{R^2} + j\omega} \tag{19}$$

This can be applied in the time domain as described in the companion paper. It could also be applied directly in the frequency domain.

5.1 Summary of procedure

This applies to various methods, including a simple lumped parameter resistance-inertance model, method of characteristics, finite element and finite difference methods.

At the start of simulation:

1. Determine limiting values Re_A and Re_B for smooth and rough flow, and values of f at these limits, using equations (2), (4), (5) and (6).
2. Determine value of σ_{CF} at Re_B using equation (10), and σ_{CW} using equation (12). Hence determine $\sigma_{WFB} = \sigma_{CF} / \sigma_{CW}$.
3. Determine cubic spline coefficients for f as described in the Appendix.
4. Estimate number of terms required using equation (39) of [1] for a typical value of σ_{CF}.

At each time step:

1. Determine low-pass filtered, spatially averaged Reynolds number Re' (equations (14)-(16)).
2. Use Re' to determine whether flow is in smooth, transition or rough region.
3. If in smooth region:
   i. determine f using equation (5);
   ii. set σ_{WF}=1, $\sigma_{CF} = \sigma_{CW}$.
   iii. determine σ_{CW} using equation (13);
4. If in transition region:
   i. determine f, from cubic spline (Appendix 2);
   ii. determine σ_{WF} by linear interpolation of logarithms between values at Re_A and Re_B, using equation (20):

$$\log_{10}(\sigma_{WF}) = z \log_{10}(\sigma_{WFB}) \tag{20}$$

   where z is given by equation (A1);

iii. determine σ_{CF} from equation (13), and calculate $\sigma_{CW} = \sigma_{CF} / \sigma_{WF}$.

5. If in rough region:
   i. determine σ_{CF} from equation (10);
   ii. determine σ_{CW} from equation (12).
6. Determine m_k^* and n_k^* from table 1 and equation (29) of [1]
7. Determine m_k and n_k from equations (14) and (15)
8. Determine weighting functions y_k using equation (35) or (36) in [1].
9. Determine friction term $h(t)$ from equation (34) in [1]

Stages 2-7 all use the filtered Reynolds number Re'.

Implementations in Matlab Simulink of various types of pipeline models incorporating this turbulent friction model are available from Johnston [10].

6. Test rig and experimental results

To validate the unsteady friction models, pressure measurements in a long pipeline with a step change in pressure or flow can be used. However it is difficult to obtain suitable experimental measurements to validate the model, as the boundary conditions and the transient input need to be as close to known and idealised conditions as possible. It is difficult to determine whether differences are due to experimental limitations or to inaccuracies in the model.

A standard test for laminar flow transients is a tube with a constant pressure reservoir at one end and a valve which is shut off rapidly at the other end. However this condition is rather an extreme test for a turbulent flow model, as the flow would undergo a complicated transition to laminar flow as it decays away. The behaviour during this transition has not been considered in this model. A test rig was needed that could provide a small, controllable step change in flow whilst maintaining turbulent flow before and after the step. A test configuration was proposed by Taylor et al [13] to achieve this, making use of symmetry. This is shown in figure 7. It consists of two long pipelines of equal length, with a bleed-off line and a fast-acting valve at the mid-point B.

It was attempted to create constant-pressure boundary conditions using gas-filled hydraulic accumulators of approximately 1 L capacity. Although the pressure in the accumulator will change as it is charged or discharged, the pressure will remain approximately constant over the short period of the measured transient. Flexible hoses were used to minimise transmission of fluid-borne noise from the pump and loading valves to the test pipeline. A three-cylinder plunger pump was used and the fluid was water. The fast-acting valve was a sliding plate valve operated using a hammer, as described by Taylor et al [13]. It was located in a side branch connected as close as possible to a tee-junction at the mid-point of the long pipeline. The fast-acting valve and the accumulators were attached rigidly to large concrete blocks with mass of approximately 200kg. The pipelines were suspended using string at intermediate points to maintain a straight line.

The test was performed by setting the fast-acting valve open initially, and setting the flow through the side branch to a small fraction of the main flow. Upon sudden closure of the fast-acting valve, a step change in flow was induced, causing waves to travel in the upstream and downstream pipeline sections. Reflections then occurred at the accumulators. This arrangement has the advantage that the dynamic behaviour of the bleed line does not have to be modelled as the fast-acting valve is closed during the transient.

The test conditions and simulation parameters are listed in table 1. The method of characteristics was used for the simulation. The turbulent transition region between smooth and rough flow was assumed to be $0.02 \le \frac{k_S u_*}{\nu_F} \le 100$, or $2660 \le Re \le 2.58 \times 10^7$. These tests were therefore in the transition region.

The experimental results were filtered using a second order Butterworth low-pass digital filter with a 1 kHz break frequency (Matlab's *filtfilt* function was used, which applies the filter in the positive and then the negative time directions, resulting in zero phase shift). Figure 8 shows the measured pressures at the pipe ends. The absolute pressure values may not be accurate due to transducer drift. It can be seen that the pressure ripple is very small (note expanded y axis) and dominated by high frequency

noise in the initial part of the transient. This noise may be due to vibration (caused by hitting the valve with the hammer) or by the non-zero inertance of the boundary conditions. The pressures also drift gradually with time due to the gradual charging of the accumulators.

Measured and simulated pressures at the mid-point B are shown in figure 9. The speed of sound in the simulations was adjusted to match the period of the measured pressure waves. It can be seen that the simulations match very well with the experimental results. Figure 10 shows the decay of the peak-to-peak pressure amplitudes at point B. There is good agreement between the decay rates for the measured and simulated results.

The simulated results in figure 9 use constant pressure boundary conditions at the ends as boundary conditions. Using the *measured* pressures as boundary conditions in the simulations gave very similar results.

Whilst the prediction of the rate of decay is clear, it is more difficult to evaluate the accuracy of the prediction of dispersion, that is, the shape of the steps. This is because the step input is not perfect, due to finite valve closure time and vibration. However the shapes of the waves do match quite well. Improved results could be obtained by using a much longer pipe to extend the wave delay time relative to the valve closure time.

The predicted flowrate just upstream of point B for test case 1 is shown in figure 11. It can be seen to be a fairly pure step, with a slight, slow drift. Immediately after the step the flowrate is 12.2 L/min, as the downstream flowrate increases by half the bleed-off flowrate and the upstream flowrate decreases by the same amount. It was not possible to measure the unsteady flowrate for comparison, but the good agreement between measured and predicted pressures in figure 9 suggests that the actual flowrate closely followed this step. This indicates that this experimental arrangement was very effective for producing a sharp, controlled flow step.

7. Flow with constant acceleration

When considering flow with a constant acceleration, Vardy and Brown [2] noted that there was some uncertainty about the determination of friction parameters at a particular Reynolds number. This is related to the time taken for the frozen viscosity distribution to adapt itself to changing conditions. He and Jackson [11] conducted an extensive series of velocity experiments on accelerating and decelerating flow in a tube. They observed that variations in the fluctuating components of the velocity were delayed relative to the levels expected for quasi-steady flow. This delay was clearest for fluctuations in the radial and circumferential components of velocity, and was greatest near the centre of the tube, reducing by a factor of two or more nearer to the walls. The delay was found to be greatest for low flowrates, so the delay reduced with time for accelerating flow and increased with time for decelerating flow.

Brown's expression for a turbulence time constant may be a simple and effective way of handling this problem. The friction terms are obtained according to the low-pass filtered Reynolds number Re'. For a flow with a constant acceleration this tends towards the value of Re delayed by a time τ_B. Equation (14) has velocity in the denominator which means that τ_B reduces with increasing velocity.

Figure 12 is reproduced from He and Jackson [11] and shows the RMS fluctuation in the radial velocity component for steady flow and for ramp flow with a ramp time of 5 seconds. This RMS fluctuation is closely related to the turbulence energy and is a good indication of the way in which the turbulence builds up during a transient. The conditions are listed in table 2. The figure shows that changes in the instantaneous fluctuation values are delayed so that the instantaneous values are less than for a steady flow at the same Reynolds number. The delay is greatest near the centre of the tube, and the delay appears to reduce as Reynolds number increases.

Simulations were performed for the same conditions as in figure 12. Wave effects were not considered in these simulations; a lumped parameter incompressible flow model was used (equation (40) in [1]). Smooth walls were assumed. Figure 13 shows the corresponding Reynolds number Re and filtered Reynolds number Re' using Brown's model, as well as the time constant τ_B. A considerable difference is apparent

depending on whether the instantaneous or filtered Reynolds number is used in equation (14), as the variations in *Re* are large in this example. In both cases however the time constant reduces with *Re*. A direct comparison with the proposed model is difficult as different quantities are being measured and modelled, and the delay in the measured RMS velocity fluctuations depends on radius, whereas in the model a single time constant is used to approximate the average development of turbulence over the whole cross-section. The near-wall development is likely to have the most effect on the pressure drop as this is where the highest velocity gradient occurs. Comparing figure 12 with figure 13, although the graphs show different quantities, similar delays are apparent, and in both cases the delays reduce with *Re*.

For accelerating flow, this gives a lower pressure drop than that predicted from the quasi-steady friction (calculated from the instantaneous flowrate). The unsteady friction terms have little effect on the results in this case. For decelerating flow, the pressure drop is higher than that predicted from quasi-steady friction.

The precise value of τ_B is important in this situation, and the approximate model proposed by Brown [9] (section 4) may need to be adjusted according to experimental measurements.

The unsteady friction terms introduce an additional pressure drop which tends towards the value given by equation (21) for low frequencies.

$$\Delta p = \frac{4\rho L\dot{q}}{A\sqrt{\sigma_{CW}}}\sum_{k=1}^{K}\frac{m_k^*}{n_k^*} \tag{21}$$

This is effectively an additional inertance term due to the non-uniform velocity profile, which adds to the inertance calculated from a uniform velocity profile (later referred to as 'simple inertance'), $\Delta p = \frac{L\dot{q}}{\rho A}$. There is a lag in the build-up of the additional term as the velocity profile develops. The ratio of this additional inertance to the simple inertance is $\frac{4}{\sqrt{\sigma_{CW}}}\sum_{k=1}^{K}\frac{m_k^*}{n_k^*}$. This ratio is plotted in figure 14. Theoretically it reaches a maximum of 1/3 for $\sigma_{CW} = 1$ (laminar flow), and reduces

with increasing σ_{CW} because the velocity profile flattens and becomes closer to the uniform velocity profile.

For flow with constant acceleration or deceleration, the dominant effects are likely to be the simple inertance and the effect of the turbulence lag on the 'steady' friction term. The pressure drop due to the unsteady friction terms (including the additional inertance) is likely to have comparatively little influence and is always much less than the pressure drop due to simple inertance. Figure 15 shows the predicted pressure drop and its components (simple inertance $\frac{\rho L}{A}$, steady friction and unsteady friction) for accelerating flow with the same conditions as figure 13 (the acceleration starts after 1 second). Both Vítkovský et al's model [12] and the proposed model for unsteady friction are shown. The instantaneous Reynolds number was used in equation (14) to calculate τ_B. In this case the inertance and steady friction are of similar magnitudes, whereas the unsteady friction is much smaller. The unsteady friction builds up from zero due to the lags in equation (16). There is a difference between the unsteady friction predicted using Vítkovský et al's model and using the proposed model; however this is a relatively small component of the overall pressure drop, and the difference in the overall pressure drops is small.

8. Conclusions

A method for predicting unsteady friction in turbulent smooth pipe flow has been extended to transitional and rough pipe flow. The method is essentially the same, but the effective wall viscosity is varied depending on Reynolds number and roughness.

An approximation has been made for the transition region by using a cubic spline for the friction factor between the smooth and rough regions. Additionally the wall viscosity is estimated using linear interpolation between the smooth and rough regions. There is considerable, inherent, uncertainty in the characteristics of the transition region because it depends on the type of roughness, that is, the surface density, height distribution, surface distribution and shape of the roughness. Also the model for smooth and fully rough flow is based on a fairly crude approximation to the viscosity profile. Therefore it is considered that the errors introduced by the transition

region approximation are likely to be sufficiently small compared to other inherent uncertainties in the transition region. The cubic spline offers greater flexibility than previous friction factor equations such as the Colebrook-White equation because the limits of the transition region can be set according to the nature of the roughness. However the unsteady friction model could also be applied in conjunction with the Colebrook-White equation or other friction factor equations.

A previously developed model for the time constant for turbulence variations has been adapted for use here, but it is recognised that this model is based on several assumptions and simplifications, and is relatively untested. It may be inaccurate in certain situations, and further work is needed to validate and possibly improve it. Notwithstanding these reservations, this makes the turbulent flow model versatile, flexible and generally applicable, as it is suitable for small and large changes in flow (where the turbulence levels change significantly), and for short and long time scales. It can also be used for laminar flow, although there is significant uncertainty during the transition between laminar and turbulent flow.

9. References

1 Johnston, D.N., Numerical modelling of unsteady turbulent flow in smooth-walled pipes, Submitted to Proc. IMechE, Part C, Journal of Mechanical Engineering Science, 2010

2 Vardy, A.E. and Brown, J.M.B., Transient turbulent friction in smooth pipe flows, Journal of Sound and Vibration, 259(5), 2003, pp1011-1036

3 Schlichting, H., Boundary Layer Theory, Seventh Edition, McGraw Hill, New York, 1979

4 Nikuradse, J., Strömungsgesetze in rauhen Rohren. Forschg. Arb. Ing.-Wes. No. 361, 1933

5 Bauer, B. and Galavics, F., Experimentelle und Theoretische Untersuchungen über die Rohrreibung von Heizwasserleitungen. Mitt. d. Fernheizkraftwerkes d. ETH, Zurich, 1939

6 Moody, L.F., Friction factors for pipe flow, Trans ASME, 66, 1944, pp671-684

7 Colebrook, C.F., Turbulent flow in pipes with particular reference to the transition region between the smooth and rough pipe laws. J Inst. Civil Engineers, 1939

8 Vardy, A.E. and Brown, J.M.B., Transient turbulent friction in fully rough pipe flows, Journal of Sound and Vibration, 270, 2004, pp233-257

9 Brown, F.T., Margolis, D.L. and Shah, R.P., Small Amplitude Frequency Behavior of Fluid Lines with Turbulent Flow, Journal of Basic Eng., Trans. ASME, December, 1969, pp678-692

10 Johnston D. N., Pipeline models in Matlab Simulink, available from http://people.bath.ac.uk/ensdnj/models, accessed Nov 2010

11 He, S. and Jackson, J.D., A study of turbulence under conditions of transient flow in a pipe, J Fluid Mech., Vol. 408, 2000, pp1-38

12 Vítkovský, J., Stephens, M., Bergant, A., Lambert, M. and Simpson, A., Efficient and accurate calculation of Zielke and Vardy-Brown unsteady friction in pipe transients, 9th International Conference on Pressure Surges, Chester, United Kingdom, 24–26 March, 2004.

13 Taylor, S. E. M., Johnston, D. N. and Longmore, D. K., Experimental validation of pipeline models for laminar and turbulent transient flow, Proceedings of the 1997 ASME International Mechanical Engineering Congress and Exposition, Dallas, TX, USA, Nov 16-21 1997, The Fluid Power and Systems Technology Division (Publication) FPST, 1997, Vol.4, pp.99- 104

Appendix 1: Notation

A Cross-sectional area

f Fanning friction factor

k Weighting function term index

k_s Effective roughness

K Number of weighting function terms

L Pipe length

m_k Weighting coefficient

n_k Weighting coefficient

N_C Core viscosity coefficient

p Pressure

q Flowrate

R Bore radius

Re Reynolds number

Re' Filtered Reynolds number

Re_A Upper limit of Reynolds number for smooth flow

Re_B Lower limit of Reynolds number for fully rough flow

W_{UE} Approximated unsteady friction function

u Fluid velocity

$\bar{u}$ Mean flow velocity over the cross-section

u_∞ Free-stream velocity

u_* Friction velocity

x Distance along pipe axis

z Interpolation variable

Δp Pressure drop

λ Darcy friction factor ($= 4f$)

ν Kinematic viscosity

ν_C Effective kinematic viscosity in core

ν_F Kinematic viscosity of fluid

ν_W Effective kinematic viscosity at wall

ρ Density

σ_{CF} Ratio of core to fluid viscosity

σ_{CW} Ratio of core to wall viscosity

σ_{WF} Ratio of wall to fluid viscosity

σ_{WFB} Ratio of wall to fluid viscosity at Re_B

τ_B Turbulence time constant

ω Angular frequency

Appendix 2: Cubic spline calculation

The following equations were used for the cubic splines. (Re_A, y_A) and (Re_B, y_B) are the ends of the spline, where $y = \log_{10}(f)$ Here a normalised independent variable z is used which is in the range from 0 to 1.

$$z = \frac{\log_{10}(Re) - \log_{10}(Re_A)}{\log_{10}(Re_B) - \log_{10}(Re_A)} \tag{A1}$$

$$y(z) = a_3 z^2 + a_2 z^2 + a_1 z + a_0 \tag{A2}$$

$$a_0 = y_A \tag{A3}$$

$$a_1 = \left.\frac{dy}{dz}\right|_{z=0} \tag{A4}$$

$$a_2 = -3y_A - 2\left.\frac{dy}{dz}\right|_{z=0} + 3y_B - \left.\frac{dy}{dz}\right|_{z=1} \tag{A5}$$

$$a_3 = 2y_A + \left.\frac{dy}{dz}\right|_{z=0} - 2y_B + \left.\frac{dy}{dz}\right|_{z=1} \tag{A6}$$

The derivatives may be calculated from the adjoining smooth and rough characteristics, equations (5) and (6).

$$\left.\frac{dy}{dx}\right|_{z=0} = \frac{\log_{10}(Re_A) - \log_{10}(Re_B)}{\frac{\log_e(10)}{8\sqrt{f}} + \frac{1}{2}} \tag{A7}$$

$$\left.\frac{dy}{dx}\right|_{z=1} = 0 \tag{A8}$$

Captions

Table 1 Test conditions and simulation parameters

Table 2 Conditions for He and Jackson's experiments [11]

Figure 1 Measured friction factor results (from Schlichting [3])

Figure 2 Resistance of commercially rough pipes (after Moody [6], reproduced from [3])

Figure 3 Nikuradse's friction factor and blended model

Figure 4 The Colebrook-White equation, Bauer and Galavics' measurements and the blended model with broader transition region

Figure 5 Variation of σ_{CW} with f for fully rough flow

Figure 6 Variation of σ_{CF}, σ_{WF} and σ_{CW} with Re

Figure 7 Experimental setup

Figure 8 Measured pressure at pipe ends
(a) Case 1, initial downstream flow = 11.2 L/min
(b) Case 2, initial downstream flow = 3.9 L/min

Figure 9 Experimental and simulated results at the mid-point
(a) Case 1, initial downstream flow = 11.2 L/min
(b) Case 2, initial downstream flow = 3.9 L/min

Figure 10 Decay of pulsations

Figure 11 Predicted flow rate just downstream of B, case 1

Figure 12 Variation of RMS fluctuation of radial velocity component for a 5 s period ramp-up flow (from [11])

Figure 13 Instantaneous and filtered Reynolds number and turbulence time constant for accelerating flow

Figure 14 Ratio of additional inertance to simple inertance

Figure 15 Pressure drop components for flow with constant acceleration

Case no.	1	2
Initial downstream flowrate	11.2 L/min	3.9 L/min
Initial bleed-off flow	2.0 L/min	2.5 L/min
Initial downstream Reynolds number	33500	11700
Speed of sound in fluid	1380 m/s	1375 m/s
Timestep	0.1826 ms	0.1833 ms
Relative roughness $\frac{k_S}{R}$	0.0002	
Fluid density	1000 kg/m^3	
Fluid viscosity	1.0 cSt	
Pipe internal diameter	7.09 mm	
Pipe wall thickness	1.22 mm	
Length from A to C	10.08 m	
Elements in MOC model between A and C	40	

Table 1 Test conditions and simulation parameters

Pipe internal diameter	50.8 mm
Pipe length	9 m
Fluid	water
Fluid density	1000 kg/m^3
Fluid viscosity	1.0 cSt
Initial flowrate	16.8 L/min
Final flowrate	108 L/min
Ramp time	5 s

Table 2 Conditions for He and Jackson's experiments [11]

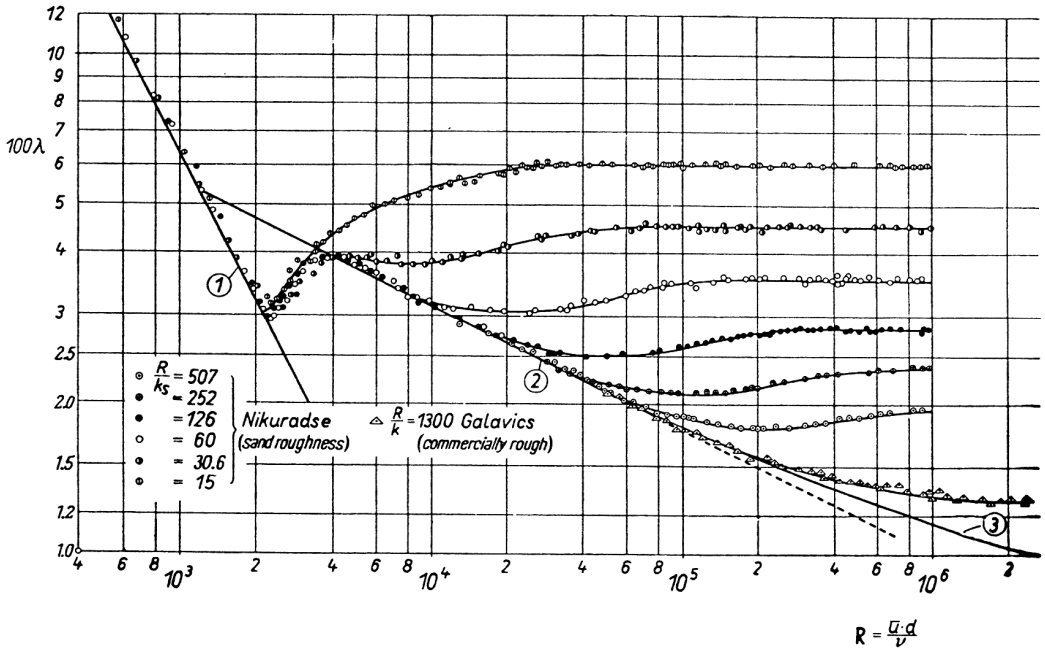

Figure 1 Measured friction factor results (from Schlichting [3])

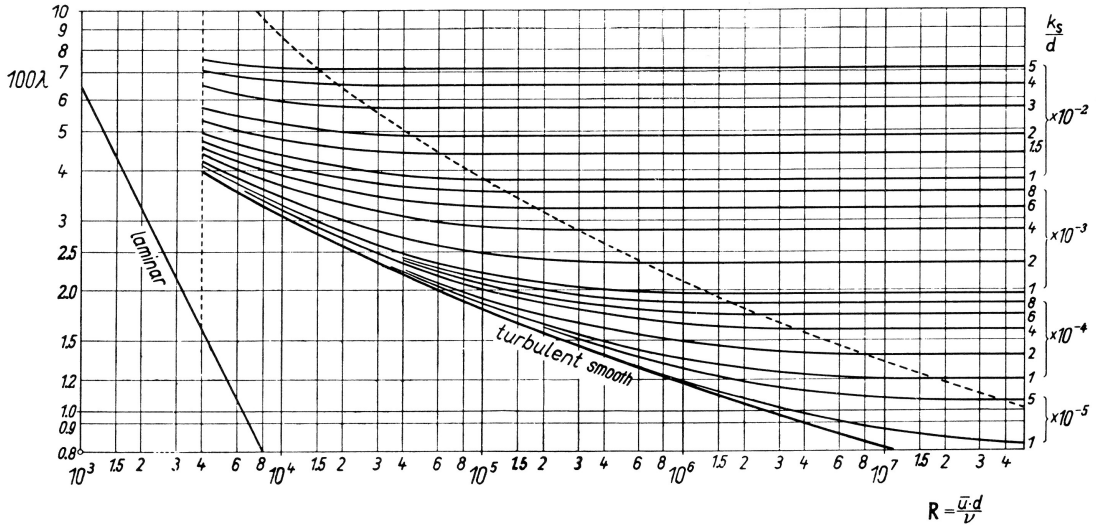

Figure 2 Resistance of commercially rough pipes (after Moody [6], reproduced from [3])

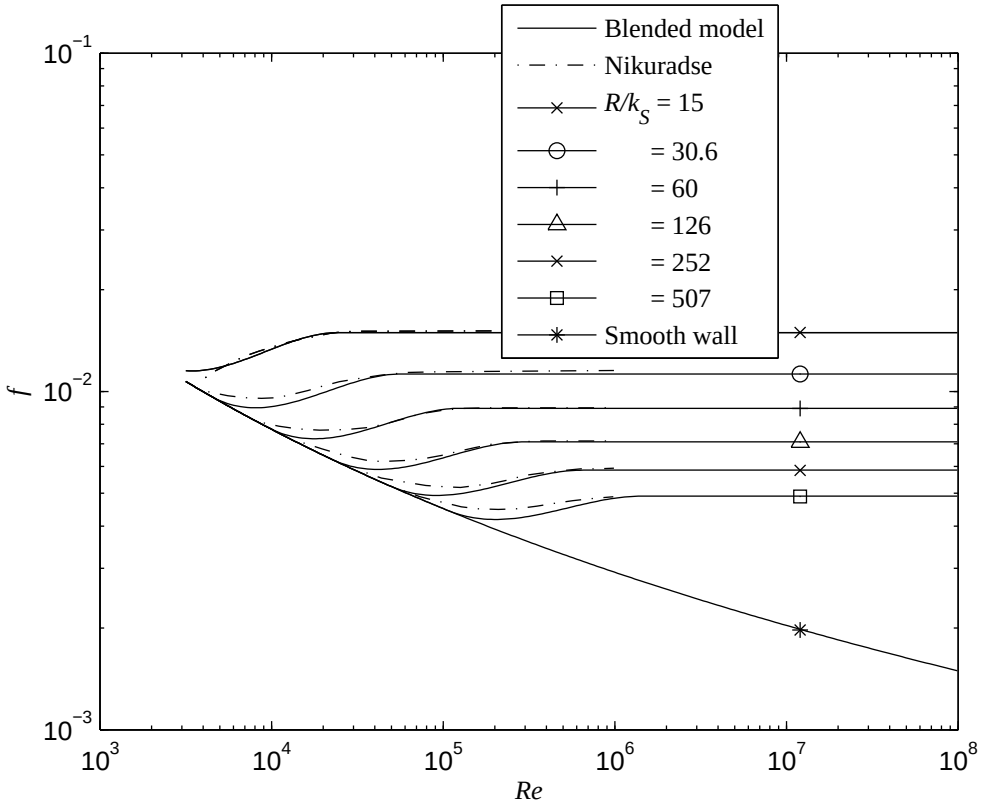

Figure 3 Nikuradse's friction factor and blended model

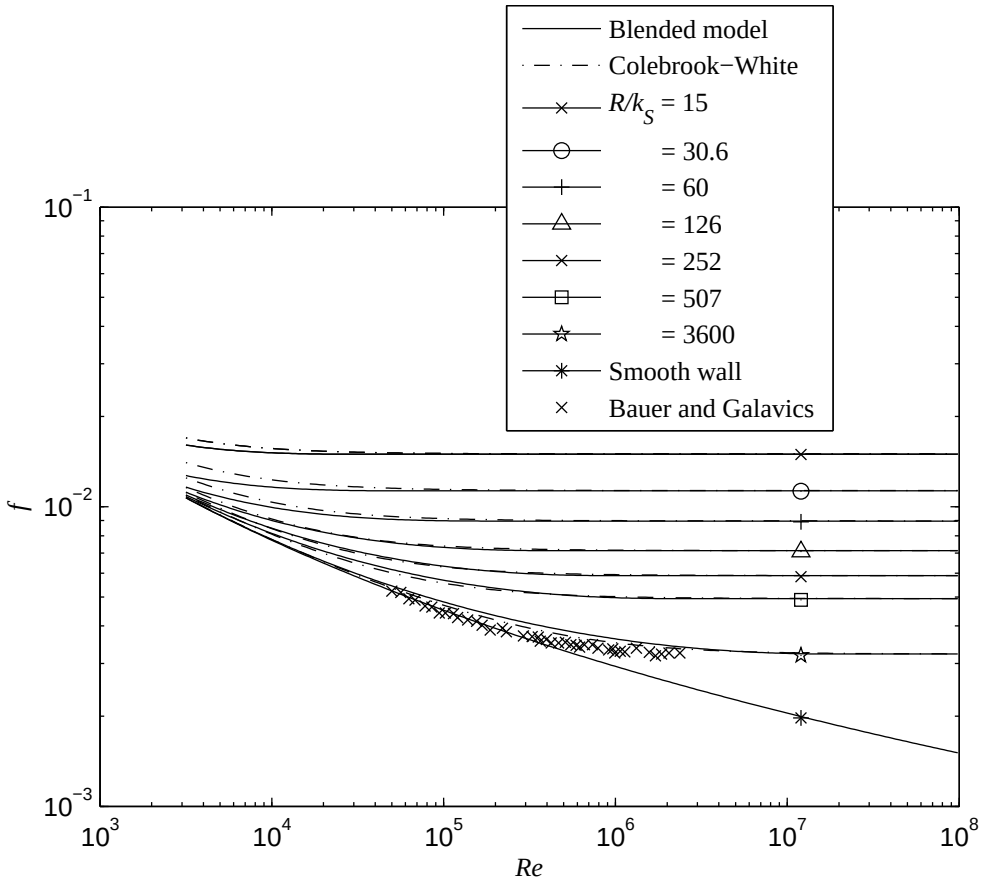

Figure 4 The Colebrook-White equation, Bauer and Galavics' measurements and the blended model with broader transition region

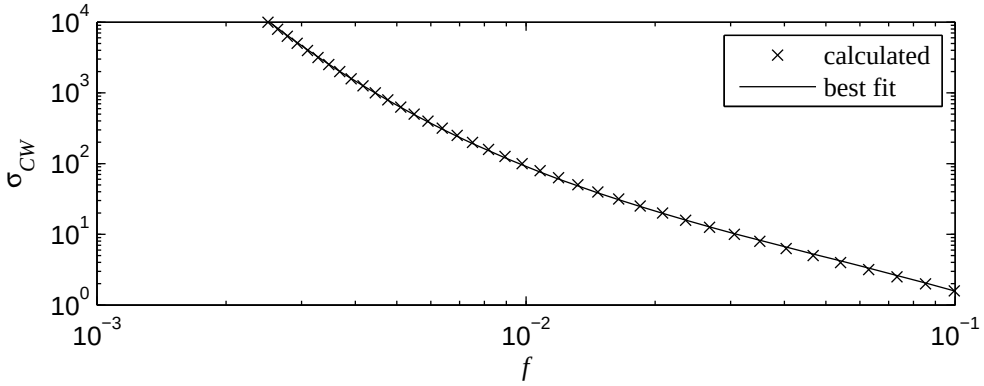

Figure 5 Variation of σ_{CW} with f for fully rough flow

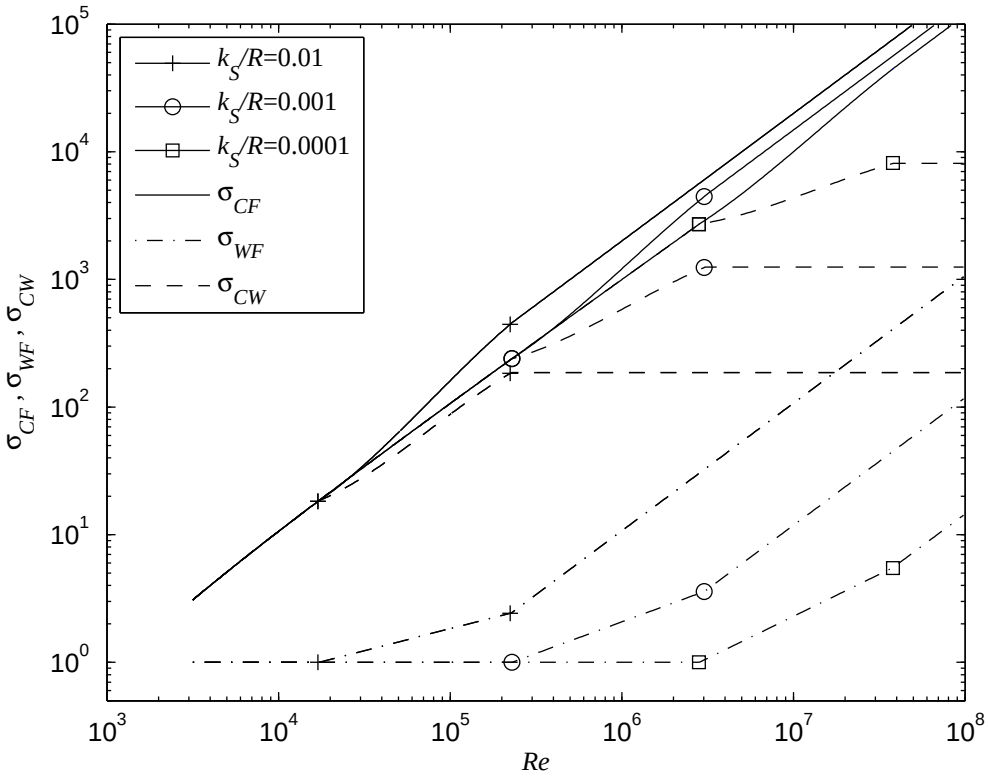

Figure 6 Variation of σ_{CF}, σ_{WF} and σ_{CW} with *Re*

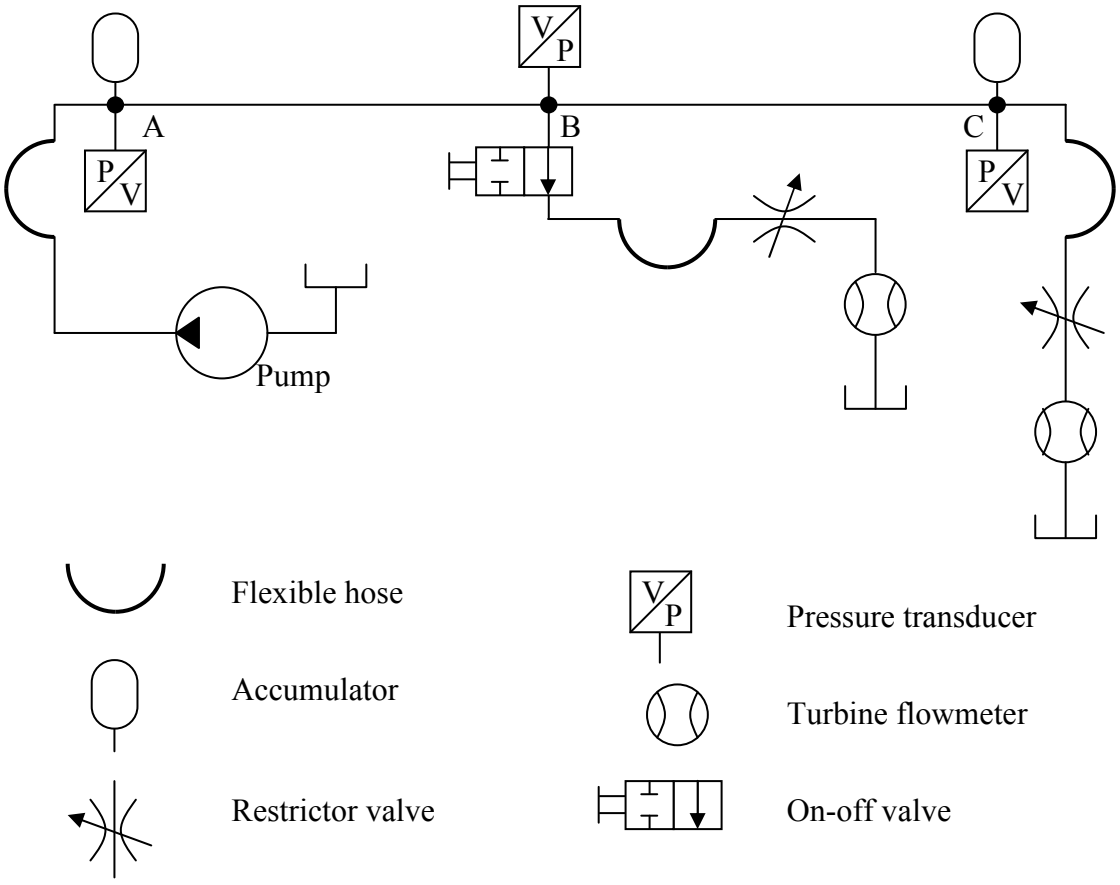

Figure 7 Experimental setup

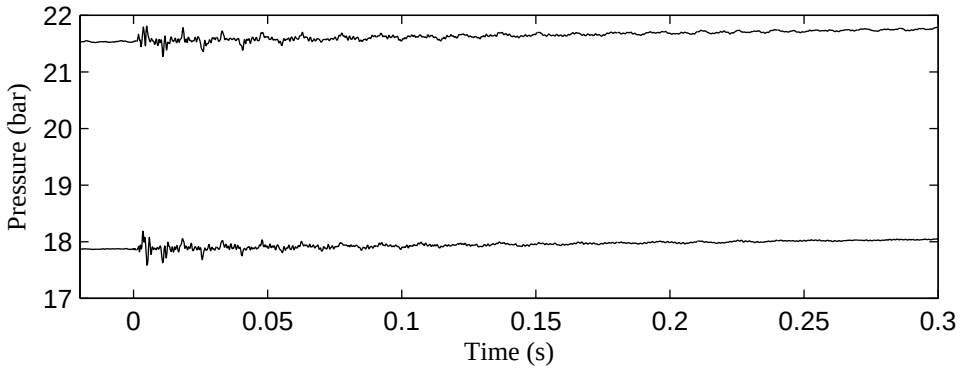

(a) Case 1, initial downstream flow = 11.2 L/min

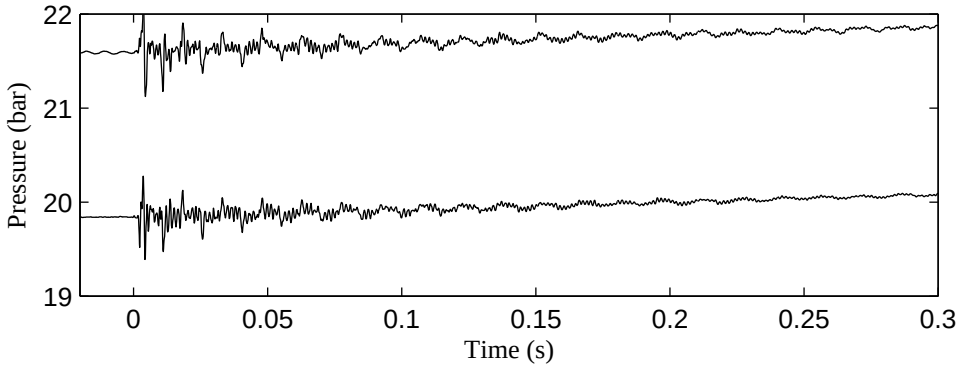

(b) Case 2, initial downstream flow = 3.9 L/min

Figure 8 Measured pressure at pipe ends

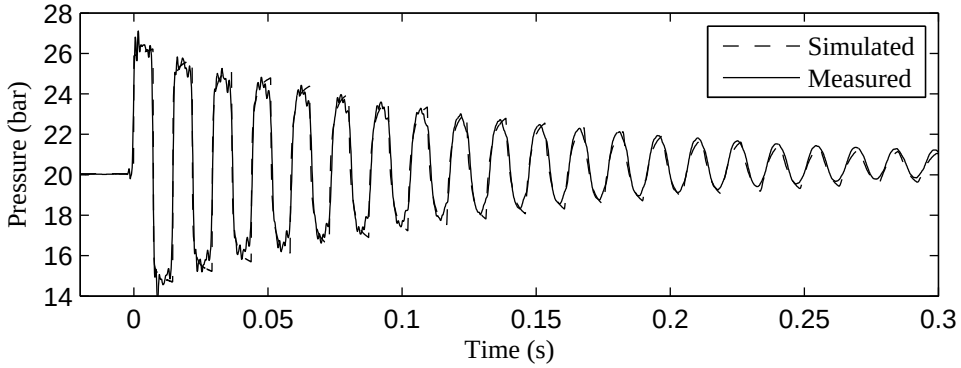

(a) Case 1, initial downstream flow = 11.2 L/min

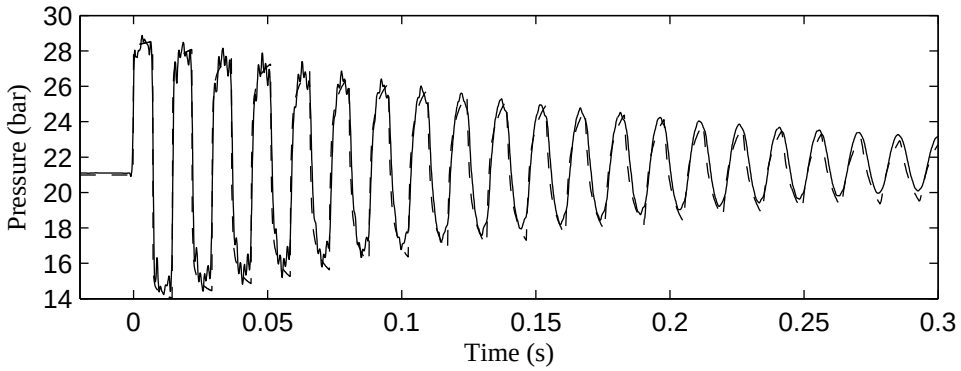

(b) Case 2, initial downstream flow = 3.9 L/min

Figure 9 Experimental and simulated results at the mid-point

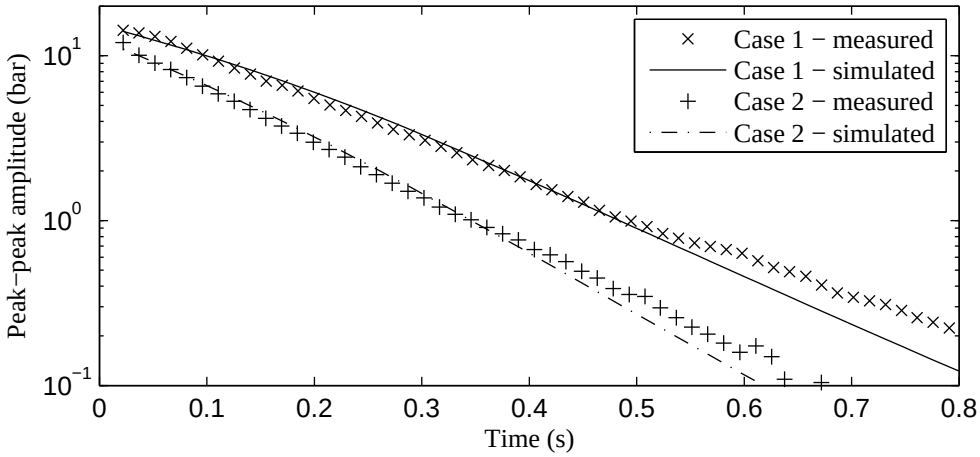

Figure 10 Decay of pulsations

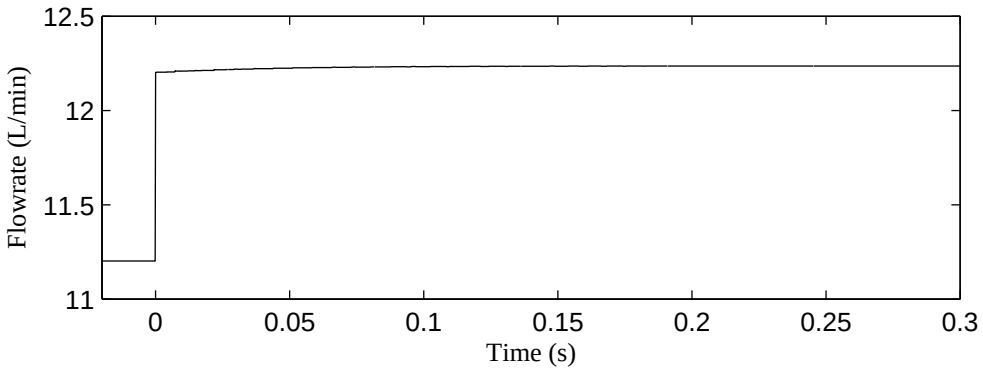

Figure 11 Predicted flow rate just downstream of B, case 1

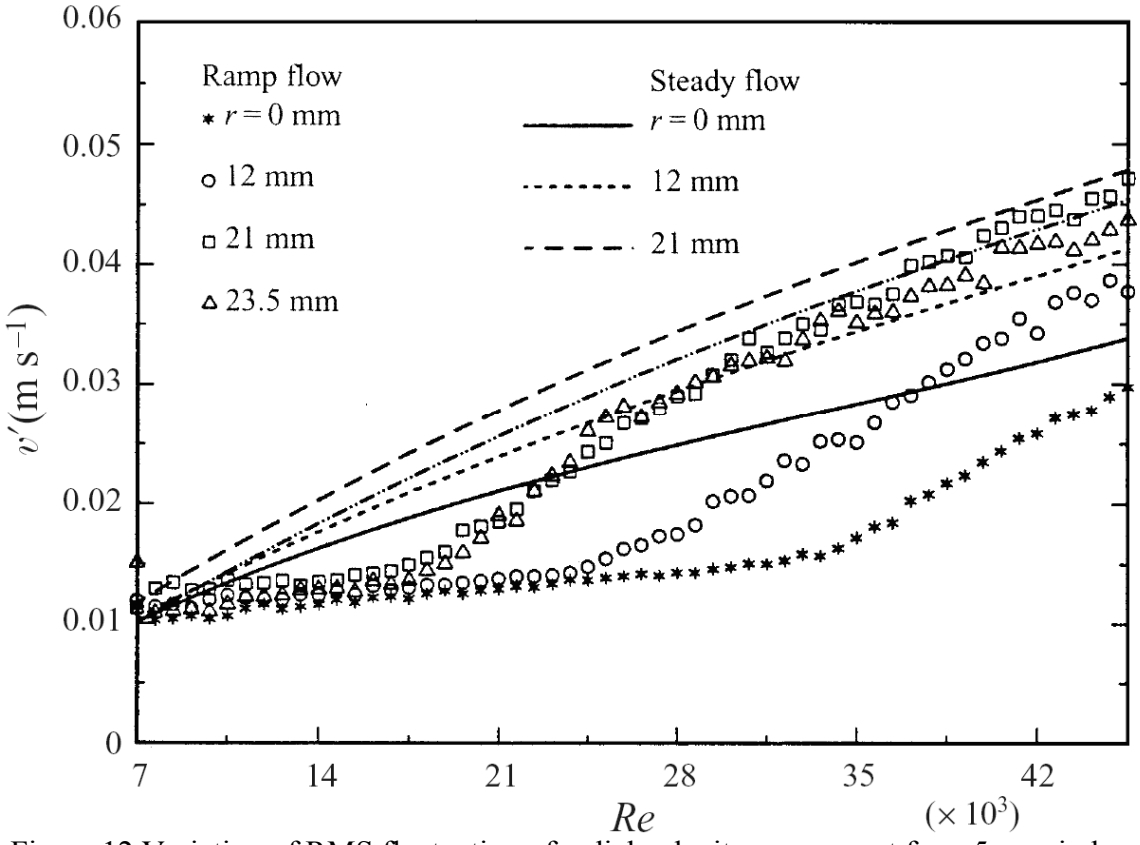

Figure 12 Variation of RMS fluctuation of radial velocity component for a 5 s period ramp-up flow (from [11])

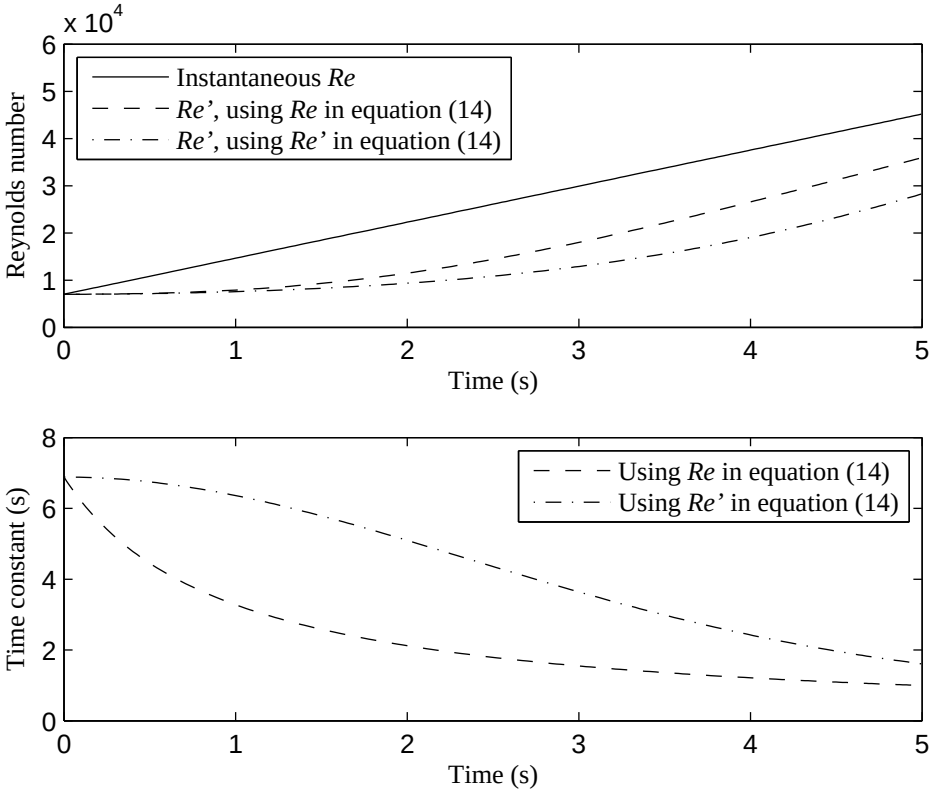

Figure 13 Instantaneous and filtered Reynolds number and turbulence time constant for accelerating flow

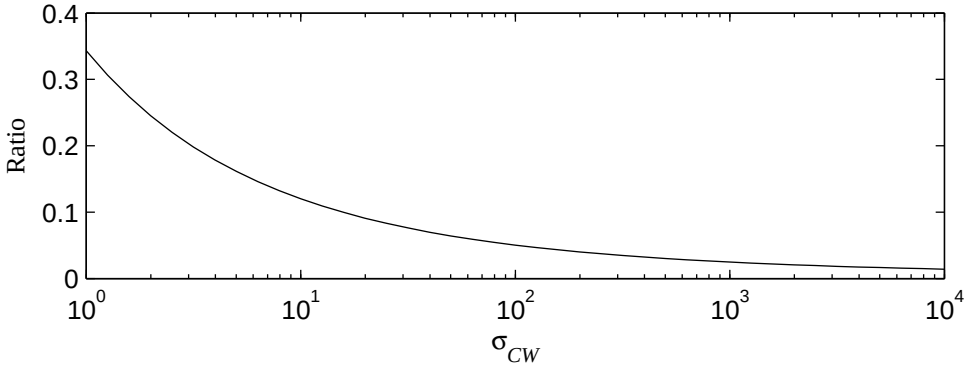

Figure 14 Ratio of additional inertance to simple inertance

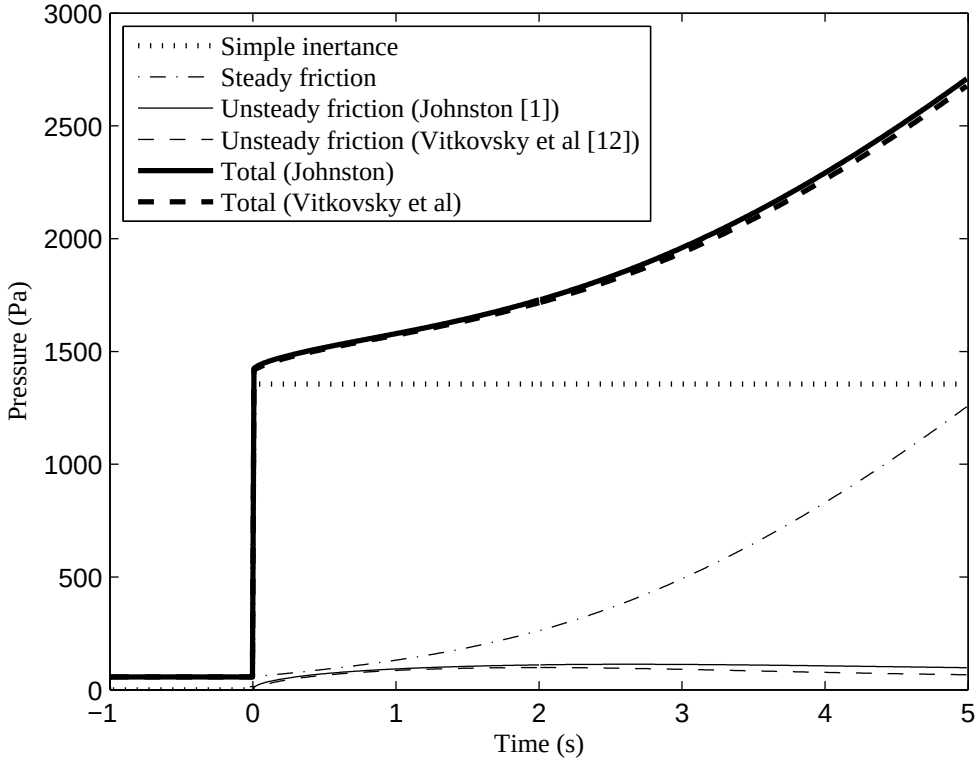

Figure 15 Pressure drop components for flow with constant acceleration